HHS Public Access

Author manuscript

Nat Nanotechnol. Author manuscript; available in PMC 2017 November 01.

Published in final edited form as:

Nat Nanotechnol. 2017 May ; 12(4): 387–393. doi:10.1038/nnano.2016.269.

Complement proteins bind to nanoparticle protein corona and undergo dynamic exchange *in vivo*

Fangfang Chen[1,2,†], **Guankui Wang**[2,†], **James I. Griffin**[2], **Barbara Brenneman**[2], **Nirmal K. Banda**[3], **V. Michael Holers**[3], **Donald S. Backos**[4], **LinPing Wu**[5], **Seyed Moein Moghimi**[5,6,7], and **Dmitri Simberg**[2,*]

[1]Department of Gastrointestinal Surgery, China-Japan Union Hospital, Jilin University, 126 Xiantai Street, Changchun, Jilin 130033, China

[2]The Skaggs School of Pharmacy and Pharmaceutical Sciences, Department of Pharmaceutical Sciences, University of Colorado Anschutz Medical Campus, 12850 East Montview Boulevard, Aurora, Colorado 80045, USA

[3]Division of Rheumatology, School of Medicine, University of Colorado Denver, Anschutz Medical Campus, 1775 Aurora Court, Aurora, Colorado 80045, USA

[4]Computational Chemistry and Biology Core Facility, the Skaggs School of Pharmacy and Pharmaceutical Sciences, Department of Pharmaceutical Sciences, University of Colorado Anschutz Medical Campus, 12850 E. Montview Boulevard, Aurora, Colorado 80045, USA

[5]Centre for Pharmaceutical Nanotechnology and Nanotoxicology, Department of Pharmacy, Faculty of Health and Medical Sciences, Universitetsparken 2, University of Copenhagen, DK-2100 Copenhagen, Denmark

[6]NanoScience Centre, University of Copenhagen, DK-2100 Copenhagen, Denmark

[7]School of Medicine, Pharmacy and Health, Durham University, Queen's Campus, Stockton-on-Tees TS17 6BH, UK

Abstract

When nanoparticles are intravenously injected into the body, complement proteins deposit on the surface of nanoparticles in a process called opsonization. These proteins prime the particle for removal by immune cells and may contribute toward infusion-related adverse effects such as allergic responses. The ways complement proteins assemble on nanoparticles have remained unclear. Here, we show that dextran-coated superparamagnetic iron oxide core-shell nanoworms

*Correspondence and requests for materials should be addressed to D.S. dmitri.simberg@ucdenver.edu.
†These authors contributed equally to this work.

Author contributions

F.C., G.W., J.I.G., B.B. and L.W. performed the experiments. D.S.B. performed complement modelling. S.M.M., N.K.B., V.M.H. and D.S. analysed the data and edited the manuscript. N.K.B. and V.M.H. provided critical reagents. S.M.M. and D.S. wrote the manuscript.

Supplementary information is available in the online version of the paper.

Competing financial interests

The authors declare no competing financial interests.

incubated in human serum and plasma are rapidly opsonized with the third complement component (C3) via the alternative pathway. Serum and plasma proteins bound to the nanoworms are mostly intercalated into the nanoworm shell. We show that C3 covalently binds to these absorbed proteins rather than the dextran shell and the protein-bound C3 undergoes dynamic exchange *in vitro*. Surface-bound proteins accelerate the assembly of the complement components of the alternative pathway on the nanoworm surface. When nanoworms pre-coated with human plasma were injected into mice, C3 and other adsorbed proteins undergo rapid loss. Our results provide important insight into dynamics of protein adsorption and complement opsonization of nanomedicines.

Intravenously injected nanoparticles in the form of contrast agents and drug carriers attract a wide range of blood proteins [1]. The composition of the blood-protein coating, which varies considerably in amount and heterogeneity, is dependent on the inherent physico-chemical properties of nanoparticles[2,3]. It has long been suggested that the protein coat may play a modulatory role in nanoparticle pharmacokinetics and biological performance[1,4,5]. There are numerous studies demonstrating the effect of isolated specific proteins on nanoparticle targeting[6], immune recognition[7] and toxicity[8]. However, considering the complexity of the blood, unravelling the role of non-specific/global protein adsorption on nanoparticle pharmacokinetic and biodistribution is a daunting task[9,10].

One example is the complement system, a critical component of the innate immunity in the blood (5% of globulins) and comprising over thirty proteins that have been consistently identified in high-throughput proteomic screens of nanoparticle coronas[2,3,5,9]. The complement system is a proteolytic cascade typically triggered via three distinct pathways (classical, lectin and alternative) that converge to generate the same set of effector molecules at the third component of complement (C3)[11]. C3 activation by pathway-specific C3 convertases generates C3b and iC3b; these species prime the surface of a nanoparticle for engulfment by leukocytes and macrophages through complement receptors[11,12]. Complement activation further liberates two potent effector molecules (C3a and C5a) that play an important role in recruitment and activation of inflammatory cells as well as anaphylaxis[13]. Numerous reports have documented pathway-specific complement activation by various types of nano-assemblies including carbon nanotubes[14,15], micelles[16], liposomes[17], polymeric nanospheres[18,19], iron oxide[20] and gold nanoparticles[21]. Despite these developments, the detailed mechanisms of complement activation and assembly on nanosurfaces remain poorly understood. In particular, although there have been many studies focused on complement activation on biomaterials and pathogens[11,22–24], the role of non-specific blood protein deposition on complement activation by nanoparticles remains unclear. For instance, adsorbed proteins may undergo conformational changes and provide domains serving as a template for complement attack[25]. This could be a non-specific and yet a predominant global mechanism accounting for complement activation by nanoparticles of different surface properties, including many long-circulating nanoparticles. Understanding these events could promote and instigate new strategies for the design and engineering of macrophage-evading and immunologically safe nanoparticles for biological targeting and drug delivery. Here, we investigate this possibility with the use of magnetic resonance

imaging contrast agent superparamagnetic iron oxide (SPIO) nanoworms consisting of a magnetite-maghemite (Fe_3O_4 and γ-Fe_2O_3) core and biopolymer dextran shell[26].

SPIO nanoworms opsonized with C3 in plasma and serum

We synthesized 20 kDa dextran-coated SPIO nanoworms[27,28] that consist of multiple crystalline iron oxide cores arranged into worm-like strings (Fig. 1a) with average length and width of the iron oxide core of 103.2 ± 38.0 nm (s.d.) and 7.0 ± 1.4 nm (s.d), respectively (Supplementary Fig. 1a and Table 1). The hydrodynamic diameter (which includes both the iron oxide core and dextran shell) is 140 ± 6.5 nm (s.d.) (Supplementary Fig. 1b and Table 1). In contrast to transmission electron microscopy (TEM), focused ion beam–scanning electron microscopy (FIB-SEM; Fig. 1a) and atomic force microscopy (AFM; Supplementary Fig. 1c) showed rounded and segmented structures. From the difference between hydrodynamic and magnetic core volumes, the average shell thickness was calculated to be 68 nm (Supplementary Table 1 and Methods). This correlates well with the length of a 20 kDa dextran molecule (120 glucose units), which is 70–80 nm in its fully extended conformation[29]. Based on gravimetric analysis (Supplementary Table 1 and Methods), each nanoworm shell contained on average 500 dextran molecules, which approaches the theoretical packing density of dextran per iron oxide core[30]. Collectively, these data suggest that SPIO nanoworms consist of a worm-like iron oxide core surrounded by a dense shell of radially projected dextran molecules, resembling a caterpillar (Fig. 1b).

Typically, the alternative pathway (AP) of the complement system (Fig. 1c) is initiated through spontaneous auto-activation (tick-over) of soluble C3 ($C3H_2O$), or when the internal thioester in the α' chain of nascent C3b reacts with hydroxyl or amino groups on a foreign surface[11]. Surface-deposited C3b leads to the formation of the surface-bound AP convertase C3bBb, which accelerates further C3 cleavage and amplification of C3b opsonization (Fig. 1c)[11]. The half-life of the C3bBb complex is greatly prolonged by the binding of properdin (P), which is present in blood at ~20 μg ml^{-1} (ref. 31). Surface-bound C3b undergoes cleavage of its α' chain by factors H and I (ref. 11), thus generating iC3b and other downstream fragments (Fig. 1d). Incubation of SPIO nanoworms in human serum or lepirudin-plasma (the anticoagulant lepirudin preserves clotting factors that are absent in serum, but does not affect the complement system like other anticoagulants) resulted in a potent opsonization with C3 fragments, mostly iC3b (Fig. 1e). Complement opsonization in serum and lepirudin plasma (hereafter just 'plasma') was completely blocked with 10 mM EDTA (an inhibitor of all pathways) or anti-properdin antibody, which inhibits AP turnover[32] (Fig. 1e). To investigate the role of C3 opsonization in immune uptake, SPIO nanoworms were incubated with serum or plasma and then added to human leucocytes. The efficiency of uptake was determined as the number of magnetically labelled leucocytes isolated over the magnetic column (see Methods). According to Fig. 1f, uptake efficiency was higher in serum than in plasma, but the uptake in both serum and plasma was significantly reduced by 10 mM EDTA, confirming the role of complement in the leucocyte uptake of SPIO nanoworms in serum and plasma.

Relationship between C3, protein corona and dextran shell

To investigate the mode of complement assembly in the context of absorbed proteins, we performed label-free liquid chromatography–mass spectrometry (LC-MS) analysis of serum and plasma proteins bound to SPIO nanoworms (Supplementary Table 2 and Supplementary section 'Mass spectrometry data'). In serum, C3, albumin, immunoglobulins and apolipoproteins were among the most abundant proteins. In plasma, fibrinogen was highly enriched on the particle surface, in addition to C3, albumin and apolipoproteins. Stoichiometric analysis of bound proteins (Supplementary Table 3, Supplementary Fig. 2 and Methods) showed ~70 and ~110 molecules of C3 bound per nanoparticle in serum and plasma, respectively. There was ~1.6 times more protein bound per particle in plasma than in serum and ~80 fibrinogen molecules per particle in plasma. Contrary to previous reports suggesting an inhibitory role of absorbed fibrinogen on complement activation[33], binding of plasma fibrinogen did not affect C3 opsonization efficiency and the pathway of activation.

In view of the extensive binding of complement and other proteins to the particles, we asked how all these proteins are accommodated on the particle surface. An earlier report suggested that proteins invade the shell of PEGylated gold nanoparticles rather than being exposed on the surface[34]. Computational modelling of C3b, C3bBb and C3bBbP (Fig. 2a) and superimposition with SPIO nanoworm average dimensions (Fig. 2b) showed that multiple AP convertases and C3b could be accommodated in the nanoworm shell. Based on the stoichiometry of serum protein binding (Supplementary Table 3), weight and volume fractions of C3 and serum proteins were determined (Fig. 2c,d). Serum proteins (including complement) constituted ~60% of the particle mass, but less than 6% (vol/vol) of the particle hydrodynamic volume. C3 constituted ~23% of particle mass, but less than 2% of particle hydrodynamic volume. The results suggest that the nanoworm dextran shell is capable of incorporating absorbed proteins, including complement factors. Indeed, particle tracking analysis and dynamic light scattering did not show any increase, but instead showed a small decrease in the size of particles after binding of serum proteins (Fig. 2e). Nor did FIB–SEM images show any change in overall particle size after binding of serum proteins (Fig. 2f and Supplementary Fig. 3a). On the other hand, TEM images revealed an accumulation of hyperintense protein clusters in close proximity to the iron oxide core (Fig. 2g and Supplementary Fig. 3b). The protein binding was heterogeneous and patchy. Notably, the protein clusters did not extend more than 50 nm outside the core, which is less than the thickness of the dextran shell. In addition, the dextran shell of nanoworms reacted with anti-dextran antibody to the same extent before and after incubation with serum (Supplementary Fig. 4 and our previous results[35]), suggesting that the adsorbed proteins do not mask the dextran shell. Collectively, these observations suggest that most of the absorbed protein is located within the dextran shell, most probably intercalated between the dextran chains.

Absorbed corona mediates binding to nanoworms

As shown in Fig. 3a, activated C3b reacts covalently with amines and hydroxyls on a foreign surface, with the formation of ester or amide bonds[36,37]. We next determined whether surface-deposited C3 is bound to protein clusters rather than to the native nanoparticle surface. Nanoparticles were incubated with serum or plasma and the proteins were eluted from nanoworms under gentle non-reducing conditions (2% SDS) to avoid the breakdown of

the covalent bond between C3 and other proteins[22]. Immunoblotting of particles treated with SDS showed that the treatment did not significantly decrease the amount of dextran on the nanoworms, but eluted over 90% of C3 (Supplementary Fig. 5), suggesting that the majority of C3 is not bound to dextran molecules. Western blot analysis of eluted C3 under non-reducing conditions (Fig. 3b) demonstrated that the majority of C3 is shifted towards a high-molecular-weight protein fraction (>250 kDa) compared with C3b or iC3b (185 kDa); it did not produce a clear band, but rather a smeared band co-localizing with high-molecular-weight proteins (Fig. 3b, silver stain). A minor fraction of C3 appeared to run similarly to iC3b under non-reducing conditions, which is probably due to self-cleavage of the covalent bond[38]. EDTA (10 mM) added to serum or plasma completely blocked C3 opsonization of nanoworms, but did not block the binding of serum or plasma proteins (Fig. 3b). These data confirm a specific attachment of C3 to the absorbed proteins. In addition to SPIO nanoworms, we performed the same experiment with 5 kDa PEGylated 30 nm gold nanoparticles (another example of a core–shell nanosystem). According to Supplementary Fig. 6, PEGylated gold nanoparticles incubated with plasma activated complement mostly via the AP, and the absorbed C3, again, was covalently bound to the absorbed proteins.

To further investigate the involvement of non-specifically adsorbed proteins in complement binding, SPIO nanoworms were incubated in normal serum, or first pre-incubated in C3-depleted serum for 30 min, then washed and incubated with reconstituted AP (RAP) factors (Fig. 4a). In a parallel experiment, SPIO nanoworms were incubated with RAP factors without precoating with serum. The activation of RAP was confirmed by cleavage of factor B (fB) and the release of fluid-phase Bb (Supplementary Fig. 7). The deposition of C3 and P on nanoworms was similar for normal serum and C3-depleted serum precoated nanoworms, but was significantly lower for nanoworms treated with RAP factors only (Fig. 4b,c). For instance, C3-depleted serum precoated nanoworms bound 2.9-fold more C3 and 2.6-fold more P than protein non-coated nanoworms. These data demonstrate that adsorbed proteins provide a scaffold for C3b binding, which could dramatically enhance the assembly of AP convertase and complement amplification compared with minor AP triggering by the native nanoworm surface.

C3 opsonization via proteins is reversible and dynamic

Classical work on protein binding to nanoparticles has demonstrated the presence of soft (dissociable) as well as hard (or non-dissociable) protein fractions[39]. In view of our results showing that the bulk of C3 is bound to proteins, we asked whether covalently bound C3 could spontaneously dissociate from the nanoworm surface. To test this, we incubated SPIO nanoworms in serum or plasma, washed and then incubated them in PBS for 1 h (Fig. 5a). According to Fig. 5b, the majority of C3 was lost from nanoworms following the incubation. The loss was not due to further degradation of surface-bound C3, as a western blot of C3 in the supernatant showed mostly iC3b and no further degradation fragments (Supplementary Fig. 8a). In addition, some of the released C3 was still bound to proteins (Supplementary Fig. 8b). P was also released into the supernatant over time (Supplementary Fig. 8c). These data suggest that surface-bound complement proteins desorb from the nanoparticle surface, probably as part of ‘soft’ protein deposits. To test whether C3 opsonization after the release is reversible, nanoworms were washed from excess proteins, incubated in PBS with shaking

for 1 h, washed, and reincubated with fresh serum or plasma from the same donor. According to Fig. 5b, SPIO nanoworms became re-opsonized with much more C3 than before the protein loss. To investigate the role of the exchangeable protein corona in immune uptake, SPIO nanoworms were incubated with serum as described above and tested for uptake by human leucocytes (see Methods). SPIO nanoworms showed efficient uptake by all types of leucocyte and predominantly by neutrophils (Fig. 5c). Serum-precoated SPIO nanoworms that were incubated with shaking for an additional 1 h before adding to leucocytes showed a 30% decrease in uptake. After secondary incubation in serum, uptake increased 1.5 times compared to washed SPIO nanoworms (Fig. 5c and Supplementary Fig. 9). These experiments demonstrate the dynamic nature of C3 opsonization, and suggest that the exchangeable fraction of complement plays a critical role in nanoparticle immune recognition.

To test whether protein-bound C3 and other absorbed proteins are exchangeable *in vivo*, we performed the following set of experiments. SPIO nanoworms were preincubated in plasma and the bound proteins were quickly labelled with IRDye 680 to minimize loss. The particles were injected intravenously, and recovered from mouse circulation (Fig. 6a). As seen in Fig. 6a (gel), the labelled proteins were quickly lost from the particles *in vivo*. To demonstrate that complement C3 is also lost from the particles, SPIO nanoworms were preincubated with human plasma (Fig. 6b) and injected into C3-deficient mouse (to avoid detection of mouse C3, which cross-reacts with human C3). According to the western blot analysis of C3 before and after injection (Fig. 6b, gel), human C3 was completely lost from the particles *in vivo*. Non-precoated SPIO nanoworms injected into wild-type mouse (Fig. 6c) became efficiently opsonized with mouse C3 (Fig. 6c, gel). These experiments demonstrate that the immunological protein corona formed around nanoparticles is kinetically unstable and undergoes dynamic exchange *in vivo*.

Conclusions

In summary, we have determined the critical role of adsorbed blood protein in the initiation and assembly of the AP of complement on core–shell nanosystems. It is still not clear which proteins (or any specific protein type) provide the most optimal surface for AP activation and binding of C3b. Immunoglobulins were enriched on SPIO nanoworms in proteomic analysis, and natural antibodies and immune complexes have been shown to provide a scaffold for complement fixation[22,40] and to trigger the AP via enhanced properdin binding[41]. The exchangeable nature of protein corona could lead to continuous shedding of complement factors and reopsonization *in vivo*. Thus, it can be hypothesized that a complement convertase shutoff mechanism (cleavage of C3b into iC3b by Factor I[42]) might not stop complement activation by circulating nanoparticles. This would be a new aspect of the *in vivo* behaviour of immunological corona, which could explain recent provocative data suggesting that nanomedicines trigger tumour growth via complement activation[43]. Moreover, continuous C3 opsonization of nanoparticles, even long-circulating species, could explain their eventual clearance by immune cells and macrophages[44,45].

Complement C3 fixation on absorbed proteins rather than on a native nanoparticle surface poses challenges to reducing complement activation by nanomedicines. One strategy could

be to minimize or completely block protein fouling. However, a PEGylated layer of nanoparticles only partially blocks protein binding, which could explain why PEGylated gold nanoparticles and other PEGylated nanoparticles[43,46] still activate complement. A more recent strategy of backfilling the gaps within the PEG layer[47] could improve anti-fouling efficiency and prevent C3 opsonization. Another strategy could be to co-administer the systemic complement inhibitor[11] or to attract natural complement inhibitors (for example, factor H[48,49]) to the nanoparticle surface. Furthermore, our data demonstrate that AP activation by nanoworms critically depends on properdin binding. Blocking properdin binding with specific antibodies[50] could be another strategy to block complement activation and immune uptake of nanoparticles. More generally, controlling protein corona composition on the nanoparticle surface could offer exciting possibilities in modulating complement activation. The basic principles uncovered in this work could offer insight to improve the safety and haemocompatibility of other nanomedicines in human subjects.

Methods

Materials

All chemical reagents used for SPIO synthesis, including iron salts and 20 kDa dextran (range 15–25 kDa) were purchased from Sigma-Aldrich. Anti-dextran DX-1 antibody (catalogue no. 10730) was purchased from StemCell Technologies. Purified human complement component C3 (catalogue no. A401), purified human complement factor B (catalogue no. A408), purified human complement factor D (catalogue no. A409), purified human complement factor P (catalogue no. A412), C3-depleted sera (catalogue no. A508) and monoclonal antibody to human factor P (catalogue no. A233) were purchased from Quidel Corporation. EGTA/Mg^{2+} (catalogue no. B106), purified human C3b (catalogue no. A114) and iC3b (catalogue no. A115) were purchased from Complement Technology. Human fibrinogen (catalogue no. 9001-32-5) was from Sigma-Aldrich. Goat anti-human and anti-mouse complement C3 polyclonal antibodies (catalogue nos. 0855117 and 0855444, respectively) were purchased from MP Biomedicals. Goat anti-mouse fibrinogen antibody, which reacts with both mouse and human fibrinogen/fibrin, was obtained from Nordic MUBio. IRDye 800CW-labelled secondary antibody anti-goat (catalogue no. 926-32214), anti-mouse (catalogue no. 926-32210) and anti-rabbit (catalogue no. 926-32213) were from Li-COR Biosciences. IRDye 680-NHS ester was from Li-COR. Copper grids (300 mesh) were purchased from Electron Microscopy Sciences. Recombinant human hirudin (lepirudin, catalogue no. ACM154) was obtained from Aniara Diagnostica, reconstituted in water to 1 μg μl^{-1} (160 antithrombin units μl^{-1}) and stored aliquoted at −80 °C. Lepirudin anticoagulated plasma (hereafter plasma) was obtained by collecting blood into a Vacutainer Z tube (catalogue no. 366408) and centrifuging the tube at 2,000*g* for 15 min. Matched human sera were obtained from the same donor by collecting blood into a Vacutainer Z tube, leaving the tube for 1 h at room temperature and centrifuging the clot at 2,500*g* for 15 min. Alternatively, human sera were purchased from Equitech-Bio. All blood products and complement proteins were kept aliquoted at −80 °C.

Synthesis of SPIO nanoworms

Nanoworms were synthesized using a one-pot Molday and MacKenzie[52] precipitation method. Nanopure water was de-oxygenated with nitrogen gas and used to dissolve 3 g dextran, 0.42 g $Fe_{(III)}$ chloride and 0.166 g $Fe_{(II)}$ chloride in a round-bottomed flask. Then, 0.75 ml of cold 25% (vol/vol) solution of ammonium hydroxide (Acros Organics) was slowly added to the mixture of dextran and iron salts under a nitrogen atmosphere with rapid stirring on ice. After the formation of nanoworms, the mixture was oil-bathed at 80 °C in the open air with stirring. After cooling, SPIO was purified overnight using a 1-MDa-dialysis bag (Spectrum Chemicals) against water to remove free dextran, followed by a washing step using a Beckman Optima ultracentrifuge (TLA-100.3 rotor, 60,000 r.p.m., 10 min). Particles were resuspended in sterile PBS, filtered through a 0.45 μm filter (Millipore) and stored at 4 °C.

Nanoparticle size and shape characterization

TEM imaging was conducted to visualize the iron oxide core using an FEI Tecnai Spirit BioTwin electron microscope (Electron Microscopy Facility at the University of Colorado Boulder). Size and zeta potential measurements of nanoparticles were determined using a Zetasizer Nano ZS (Malvern Instruments). The intensity weighted size distribution peak value was used to report hydrodynamic diameters of nanowires. For some samples, the number weighted diameter was measured with a particle tracking analysis instrument NanoSight (Malvern Instruments). For simplicity, the absolute count of cells in each size bin (*y* axis) was converted to a percentage of cells. AFM was performed at the Nanomaterials Characterization Facility, University of Colorado Boulder. Highly diluted samples were dried on a cleaned borosilicate glass surface and imaged using a Nanosurf EasyScan 2 AFM (110 μm scan head) with an Aspire Conical AFM probe tip (CT170R) using intermittent contact (dynamic force mode) to avoid damage to the samples. FIB–SEM was used to visualize overall particle shape (including the shell) with an FEI Nova 600 Nanolab Dual Beam System equipped with a Schottky field emitter. Samples were dried on a piece of silicon substrate and coated with carbon to avoid charging. The stage was tiled to 52° during the observation and imaged at an accelerating voltage of 5 kV.

Nanoparticle chemical composition

Nanoworm concentration per milligram Fe was determined with a NanoSight (Malvern Instruments) and Fe concentration was determined with a ferrozine iron assay as described previously[53]. Theoretical particle concentration was estimated as described previously[54] based on the number of Fe atoms per 7 nm crystal (~11,000) and ~20 crystals per SPIO nanoworm. The theoretical concentration was higher than that determined with the NanoSight (4.88×10^{13} versus 3.99×10^{13}), and NanoSight concentration was used in all calculations. The shell volume was determined from the average TEM dimensions of the iron oxide core and dynamic light scattering (DLS) measurements of hydrodynamic diameter as described before[30,55]. Briefly, the iron oxide core volume was calculated based on contour length and width (length × width × width). These dimensions were determined from TEM images taken at high (100,000–340,000) magnification. At least 100 cores were counted. The data were plotted as frequency histograms using GraphPad to determine the

mean length and width. Hydrodynamic volume was calculated as the volume of a sphere using the DLS diameter. Shell volume was determined as the difference between the hydrodynamic volume and the core volume. The number of dextran chains per nanoworm was determined by gravimetric analysis (performed twice). Freshly made particles (40 mg Fe in 1 ml) were dialysed in double-distilled water (DDW) overnight, washed three times in DDW by ultracentrifugation to remove any residual dextran. After the last wash, particles were precipitated in *tert*-butanol, centrifuged again to remove the solvent and residual water, and the pellet was lyophilized overnight to completely dry the pellet. To ensure there was no residual water left in the pellet, the latter was further dried at 100 °C for 2 h. The weight of the pellet was accurately measured and the dry weight of the dextran shell was calculated by subtracting the weight of the crystal Fe_3O_4 weight (which was calculated from the Fe weight in the pellet). The number of dextran molecules per particle, N_d, was calculated as

$$N_d = \frac{W_d \times N_A}{(20,000\,\mathrm{Da} \times N_p)}$$

where W_d is the dry weight of the dextran shell, N_A is the Avogadro number and N_p is the number of nanoparticles in the pellet (determined as described above). Chloride content was assayed with an $AgNO_3$ titration agent (Sigma-Aldrich) after dissolving the pellet in concentrated nitric acid and was determined to be below the detection level.

Analysis of binding of proteins to particles

Experiments with human serum and plasma were performed under exemption from the Colorado Multiple Institutional Review Board (IRB) protocol because the samples were completely de-identified. For a binding assay of complement C3, 1 mg ml^{-1} (Fe) SPIO nanowire solution in PBS was mixed with human serum or lepirudin plasma at a 1:3 (vol/vol) ratio in the presence or absence of complement inhibitors (10 mM EDTA, 10 mM EGTA/Mg^{2+} or anti-properdin antibody (1:10 dilution). At the end of incubation (37 °C, 30 min), particles were washed three times by centrifugation at 60,000 r.p.m. at 4 °C in Ca^{2+}/Mg^{2+}-supplemented PBS using a Beckman Optima TLX ultracentrifuge. The pellets were resuspended in 20 μl PBS, separated with SDS–PAGE under reducing conditions and analysed by western blot for bound C3. For quantification of absorbed C3 and fibrinogen, the protein corona was eluted by incubating nanoparticles with 2% SDS and quantified with a dot-blot assay as follows. For each sample, 2 μl aliquots were applied in a triplicate onto a 0.45-μm-pore nitrocellulose membrane (Bio-Rad). The membranes were blocked using 5% (wt/wt) non-fat dry milk in PBS-T (1× PBS with 0.1% Tween 20) for 1 h at room temperature, probed with corresponding primary antibodies for 1 h at room temperature, followed by washing the membranes three times with PBS-T and finally 1 h incubation with the corresponding IRDye 800CW-labelled secondary antibodies against the primary antibody species. The signal was visualized using an Odyssey infrared imager (Li-COR Biosciences). The integrated dot intensity in the scanned images was determined from 16-bit greyscale images using ImageJ software and plotted using Prism 6 software (GraphPad Software). The number of C3 and fibrinogen molecules per spot was determined from the standard dilutions of corresponding purified proteins applied to the membrane and the

number of protein molecules per particle was subsequently determined by dividing the number of protein molecules by the number of nanoparticles applied per spot (Supplementary Fig. 2). The amount of protein per nanoworm was determined by measuring the total eluted protein with a Bio-Rad BCA assay against albumin standard prepared in 2% SDS/PBS. The volume of C3 was calculated from the mass of these proteins per particle and the protein packing parameter 0.73 ml g^{-1} (ref. 56); the loose volume of proteins was determined by dividing the mass of proteins per particle by the blood serum density (1.025 g m^{-3}). Serum density was used to determine the maximum volume occupied by proteins. This density is lower than the density calculated from the protein packing parameter (1.363 g ml^{-1}) or the reported dried protein density of 1.22 g ml^{-1} (ref. 57). In the case of protein being densely packed inside the particles, a higher density should be used.

Proteomic identification of SPIO nanoworm-binding proteins

Particles (200 μl, 1 mg Fe per ml) were incubated with human serum or plasma (600 μl) as described above. After washing three times with 1 ml PBS, the proteins were eluted from particles with 2% SDS in PBS for 1 h, the particles were pelleted by ultracentrifuge, and the supernatant was submitted to the proteomics and Metabolomics core facility at the Skaggs School of Pharmacy. A filter-aided sample preparation method was used[58]. The sample was analysed with a C-18 reverse-phase nano LC column (100 μm × 150 mm, 3.0 μm, 200A; ProntoSil C18AQ by Nano LCMS Solutions). The sample was loaded onto a trap column of the same packing material for 5 min at 10 μl min^{-1} before the elution gradient was started. The elution gradient was a 5–50% buffer B for 60 min at a flow rate of 800 nl min^{-1}. A Bruker Impact HD Q-TOF mass spectrometer was used to analyse the sample. One microlitre of sample was injected. MS data were acquired in triplicates using the nano-booster mode with the following parameters: mass range of 150–2,200 *m*/*z*, scan rate of 2.0 Hz, precursor cycle time of 3.0 s, absolute threshold of 500 counts, 0% relative threshold, exclude after one spectrum and release after 2 min and reconsider precursor if the ratio of the current intensity to the previous intensity is 3.0. The MS/MS spectra were searched against the Swiss-Prot human database with ProteinScape 3.0 (Bruker) using Mascot software. Trypsin cleavage specificity was set with a maximum of two missed cleavages allowed and variable cysteinyl carbamidomethylation, deamidation (NQ) and oxidized methionine modifications were allowed. Peptide tolerance was set to 10.0 ppm and a MS/MS tolerance to 0.5 Da. Peptides must be at least five amino acids long and proteins were accepted if they had a mascot score of >40 and peptides were accepted if they had a mascot score >20.

SPIO nanoworm uptake by human leukocytes

For uptake experiments, fresh K_2EDTA anticoagulated blood from a healthy female volunteer was obtained from Colorado Blood Bank. The uptake was studied as described previously[59]. Briefly, blood cells (leukocytes, RBCs) were washed with 1% (wt/vol) BSA–PBS three times to remove anticoagulated plasma and then washed once with PBS to remove BSA. Particles were incubated with human sera or plasma at 37 °C for 30 min. For complement inhibition, EDTA (10 mM) was added to serum/plasma for 15 min at room temperature before the addition of SPIO nanoworms. Particles were washed as described above and incubated with leucocytes at 37 °C for 1 h at 500 r.p.m. (Thermomixer,

Eppendorf). The blood cells were then washed with PBS to remove the nanoparticles and the cells with internalized particles were separated using Mini MACS magnetic columns (Miltenyi Biotec). Eluted cells from different groups were suspended in equal amounts of 1% (wt/vol) BSA–PBS and concentrated on glass slides using cytospin (Thermo Fisher Scientific). The slides were then fixed with 10% buffered formalin solution and stained with Hoechst nuclear stain (Thermo Fisher). Between 10 and 20 random microscopic areas were used for leucocyte counting.

Modelling of complement proteins

Crystal structure coordinates for the C3bBb complex[60] and the properdin trimer were downloaded from the Protein Data Bank (PDB ID: 2XWB and 1W0S, respectively). Protein structures were prepared, measured and visualized using Biovia Discovery Studio 4.5 (Biovia). A complex of P trimer with three C3b and three Bb molecules was modelled based on published electron microscopy data[31].

In vivo experiments

Mouse studies were performed under the University of Colorado IACUC-approved protocol according to the institutional guidelines for animal care. No randomization or blinding was done for animal experiments. Female wild-type and C3 knockout mice (C57BL/6) were bred in-house and used at the age of 8 weeks. To label proteins bound to SPIO nanoworms while minimizing protein loss, nanoparticles (200 μg iron) were pre-incubated in 600 μl human plasma as described above, pelleted once by ultracentrifuge and labelled with IRDye 680 NHS ester for 15 min. Following the labelling procedure, the particles were washed twice in PBS and injected into C3-sufficient or C3-deficient mice. Blood (1 ml) was collected 5 min post-injection through cardiac puncture using heparin as anticoagulant and quickly separated on a MIDI MACS magnetic column. The particles were eluted, concentrated, boiled in reducing SDS–PAGE buffer and separated with 4–20% SDS–PAGE. The proteins were transferred to nitrocellulose membrane and scanned with an Odyssey scanner at 700 nm channel to visualize the fluorescently labelled proteins. Alternatively, the membranes were probed for mouse or human C3 as described above.

Statistical analysis

All differences between samples were compared by non-paired two-tailed Student's parametric *t*-test assuming 95% confidence interval. The *P* value was calculated by Prizm (GraphPad). For animal non-quantitative experiments, the sample size of two was deemed sufficient to verify the loss of complement proteins *in vivo*.

Supplementary Material

Refer to Web version on PubMed Central for supplementary material.

Acknowledgments

The study was funded by the University of Colorado Denver start-up funding and NIH 1R01EB022040 to D.S. F.C. was supported by the International Postdoctoral Exchange Fellowship Program (2013) from China Postdoctoral Council. Molecular modelling studies were conducted at the University of Colorado Computational Chemistry and

Biology Core Facility, which is supported in part by NIH/NCATS Colorado CTSA grant no. UL1 TR001082. S.M.M. acknowledges financial support by the Danish Agency for Science, Technology and Innovation (Det Strategiske Forskningsråd), reference 09-065746, and Technology and Production, reference 12-126894.

References

1. Moghimi SM, Hunter AC, Andresen TL. Factors controlling nanoparticle pharmacokinetics: an integrated analysis and perspective. Annu Rev Pharmacol Toxicol. 2012; 52:481–503. [PubMed: 22035254]
2. Blunk T, Hochstrasser DF, Sanchez JC, Muller BW, Muller RH. Colloidal carriers for intravenous drug targeting—plasma-protein adsorption patterns on surface-modified latex-particles evaluated by 2-dimensional polyacrylamide-gel electrophoresis. Electrophoresis. 1993; 14:1382–1387. [PubMed: 8137807]
3. Lundqvist M, et al. Nanoparticle size and surface properties determine the protein corona with possible implications for biological impacts. Proc Natl Acad Sci USA. 2008; 105:14265–14270. [PubMed: 18809927]
4. Chonn A, Semple SC, Cullis PR. Association of blood proteins with large unilamellar liposomes *in vivo*. Relation to circulation lifetimes. J Biol Chem. 1992; 267:18759–18765. [PubMed: 1527006]
5. Tenzer S, et al. Rapid formation of plasma protein corona critically affects nanoparticle pathophysiology. Nat Nanotech. 2013; 8:772–781.
6. Salvati A, et al. Transferrin-functionalized nanoparticles lose their targeting capabilities when a biomolecule corona adsorbs on the surface. Nat Nanotech. 2013; 8:137–143.
7. Mortimer GM, et al. Cryptic epitopes of albumin determine mononuclear phagocyte system clearance of nanomaterials. ACS Nano. 2014; 8:3357–3366. [PubMed: 24617595]
8. Deng ZJ, Liang M, Monteiro M, Toth I, Minchin RF. Nanoparticle-induced unfolding of fibrinogen promotes Mac-1 receptor activation and inflammation. Nat Nanotech. 2011; 6:39–44.
9. Walkey CD, et al. Protein corona fingerprinting predicts the cellular interaction of gold and silver nanoparticles. ACS Nano. 2014; 8:2439–2455. [PubMed: 24517450]
10. Karmali PP, Simberg D. Interactions of nanoparticles with plasma proteins: implication on clearance and toxicity of drug delivery systems. Exp Opin Drug Deliv. 2011; 8:343–357.
11. Ricklin D, Hajishengallis G, Yang K, Lambris JD. Complement: a key system for immune surveillance and homeostasis. Nat Immunol. 2010; 11:785–797. [PubMed: 20720586]
12. Moghimi SM, Szebeni J. Stealth liposomes and long circulating nanoparticles: critical issues in pharmacokinetics, opsonization and protein-binding properties. Prog Lipid Res. 2003; 42:463–478. [PubMed: 14559067]
13. Moghimi SM, et al. Complement activation cascade triggered by PEG-PL engineered nanomedicines and carbon nanotubes: the challenges ahead. J Control Rel. 2010; 146:175–181.
14. Salvador-Morales C, et al. Complement activation and protein adsorption by carbon nanotubes. Mol Immunol. 2006; 43:193–201. [PubMed: 16199256]
15. Andersen AJ, et al. Single-walled carbon nanotube surface control of complement recognition and activation. ACS Nano. 2013; 7:1108–1119. [PubMed: 23301860]
16. Hamad I, Hunter AC, Moghimi SM. Complement monitoring of Pluronic 127 gel and micelles: suppression of copolymer-mediated complement activation by elevated serum levels of HDL, LDL, and apolipoproteins AI and B-100. J Control Rel. 2013; 170:167–174.
17. Devine DV, Wong K, Serrano K, Chonn A, Cullis PR. Liposome–complement interactions in rat serum: implications for liposome survival studies. Biochim Biophys Acta. 1994; 1191:43–51. [PubMed: 8155683]
18. Borchard G, Kreuter J. The role of serum complement on the organ distribution of intravenously administered poly(methyl methacrylate) nanoparticles: effects of pre-coating with plasma and with serum complement. Pharm Res. 1996; 13:1055–1058. [PubMed: 8842044]
19. Hamad I, et al. Distinct polymer architecture mediates switching of complement activation pathways at the nanosphere–serum interface: implications for stealth nanoparticle engineering. Acs Nano. 2010; 4:6629–6638. [PubMed: 21028845]

20. Pedersen MB, et al. Curvature of synthetic and natural surfaces is an important target feature in classical pathway complement activation. J Immunol. 2010; 184:1931–1945. [PubMed: 20053940]
21. Dobrovolskaia MA, et al. Interaction of colloidal gold nanoparticles with human blood: effects on particle size and analysis of plasma protein binding profiles. Nanomedicine. 2009; 5:106–117. [PubMed: 19071065]
22. Andersson J, Ekdahl KN, Lambris JD, Nilsson B. Binding of C3 fragments on top of adsorbed plasma proteins during complement activation on a model biomaterial surface. Biomaterials. 2005; 26:1477–1485. [PubMed: 15522749]
23. Andersson J, Ekdahl KN, Larsson R, Nilsson UR, Nilsson B. C3 adsorbed to a polymer surface can form an initiating alternative pathway convertase. J Immunol. 2002; 168:5786–5791. [PubMed: 12023380]
24. Hong J, Azens A, Ekdahl KN, Granqvist CG, Nilsson B. Material-specific thrombin generation following contact between metal surfaces and whole blood. Biomaterials. 2005; 26:1397–1403. [PubMed: 15482827]
25. Gbadamosi JK, Hunter AC, Moghimi SM. PEGylation of microspheres generates a heterogeneous population of particles with differential surface characteristics and biological performance. FEBS Lett. 2002; 532:338–344. [PubMed: 12482589]
26. Gupta AK, Gupta M. Synthesis and surface engineering of iron oxide nanoparticles for biomedical applications. Biomaterials. 2005; 26:3995–4021. [PubMed: 15626447]
27. Park JH, et al. Systematic surface engineering of magnetic nanoworms for *in vivo* tumor targeting. Small. 2009; 5:694–700. [PubMed: 19263431]
28. Park JH, et al. Magnetic iron oxide nanoworms for tumor targeting and imaging. Adv Mater. 2008; 20:1630–1635. [PubMed: 21687830]
29. Kawaguchi T, Hasegawa M. Structure of dextran–magnetite complex: relation between conformation of dextran chains covering core and its molecular weight. J Mater Sci Mater Med. 2000; 11:31–35. [PubMed: 15348096]
30. Jung CW. Surface properties of superparamagnetic iron oxide MR contrast agents: ferumoxides, ferumoxtran, ferumoxsil. Magn Reson Imaging. 1995; 13:675–691. [PubMed: 8569442]
31. Alcorlo M, Tortajada A, Rodriguez de Cordoba S, Llorca O. Structural basis for the stabilization of the complement alternative pathway C3 convertase by properdin. Proc Natl Acad Sci USA. 2013; 110:13504–13509. [PubMed: 23901101]
32. Gupta-Bansal R, Parent JB, Brunden KR. Inhibition of complement alternative pathway function with anti-properdin monoclonal antibodies. Mol Immunol. 2000; 37:191–201. [PubMed: 10930626]
33. Carlsson F, Sandin C, Lindahl G. Human fibrinogen bound to *Streptococcus pyogenes* M protein inhibits complement deposition via the classical pathway. Mol Microbiol. 2005; 56:28–39. [PubMed: 15773976]
34. Pelaz B, et al. Surface functionalization of nanoparticles with polyethylene glycol: effects on protein adsorption and cellular uptake. ACS Nano. 2015; 9:6996–7008. [PubMed: 26079146]
35. Simberg D, et al. Differential proteomics analysis of the surface heterogeneity of dextran iron oxide nanoparticles and the implications for their *in vivo* clearance. Biomaterials. 2009; 30:3926–3933. [PubMed: 19394687]
36. Arima Y, Kawagoe M, Toda M, Iwata H. Complement activation by polymers carrying hydroxyl groups. ACS Appl Mater Interfaces. 2009; 1:2400–2407. [PubMed: 20355878]
37. Lemarchand C, et al. Influence of polysaccharide coating on the interactions of nanoparticles with biological systems. Biomaterials. 2006; 27:108–118. [PubMed: 16118015]
38. Venkatesh YP, Minich TM, Law SK, Levine RP. Natural release of covalently bound C3b from cell surfaces and the study of this phenomenon in the fluid-phase system. J Immunol. 1984; 132:1435–1439. [PubMed: 6693771]
39. Cedervall T, et al. Understanding the nanoparticle–protein corona using methods to quantify exchange rates and affinities of proteins for nanoparticles. Proc Natl Acad Sci USA. 2007; 104:2050–2055. [PubMed: 17267609]

40. Gadd KJ, Reid KB. The binding of complement component C3 to antibody–antigen aggregates after activation of the alternative pathway in human serum. Biochem J. 1981; 195:471–480. [PubMed: 7316962]
41. Zhou HF, et al. Antibody directs properdin-dependent activation of the complement alternative pathway in a mouse model of abdominal aortic aneurysm. Proc Natl Acad Sci USA. 2012; 109:E415–E422. [PubMed: 22308431]
42. Zipfel PF, Skerka C. Complement regulators and inhibitory proteins. Nat Rev Immunol. 2009; 9:729–740. [PubMed: 19730437]
43. Moghimi SM. Cancer nanomedicine and the complement system activation paradigm: anaphylaxis and tumour growth. J Control Rel. 2014; 190:556–562.
44. Zamboni WC, et al. Bidirectional pharmacodynamic interaction between pegylated liposomal CKD-602 (S-CKD602) and monocytes in patients with refractory solid tumors. J Liposome Res. 2011; 21:158–165. [PubMed: 20626314]
45. Moghimi SM, Hunter AC, Murray JC. Long-circulating and target-specific nanoparticles: theory to practice. Pharmacol Rev. 2001; 53:283–318. [PubMed: 11356986]
46. Hamada I, Hunter AC, Szebeni J, Moghimi SM. Poly(ethylene glycol)s generate complement activation products in human serum through increased alternative pathway turnover and a MASP-2-dependent process. Mol Immunol. 2008; 46:225–232. [PubMed: 18849076]
47. Dai Q, Walkey C, Chan WC. Polyethylene glycol backfilling mitigates the negative impact of the protein corona on nanoparticle cell targeting. Angew Chem Int Ed. 2014; 53:5093–5096.
48. Wu YQ, et al. Protection of nonself surfaces from complement attack by factor H-binding peptides: implications for therapeutic medicine. J Immunol. 2011; 186:4269–4277. [PubMed: 21339361]
49. Thomas SN, et al. Engineering complement activation on polypropylene sulfide vaccine nanoparticles. Biomaterials. 2011; 32:2194–2203. [PubMed: 21183216]
50. Pauly D, et al. A novel antibody against human properdin inhibits the alternative complement system and specifically detects properdin from blood samples. PLoS ONE. 2014; 9:e96371. [PubMed: 24797388]
51. Kozel TR, Wilson MA, Pfrommer GS, Schlageter AM. Activation and binding of opsonic fragments of C3 on encapsulated *Cryptococcus neoformans* by using an alternative complement pathway reconstituted from six isolated proteins. Infect Immun. 1989; 57:1922–1927. [PubMed: 2525113]
52. Molday RS, MacKenzie D. Immunospecific ferromagnetic iron–dextran reagents for the labeling and magnetic separation of cells. J Immunol Methods. 1982; 52:353–367. [PubMed: 7130710]
53. Wang G, et al. High-relaxivity superparamagnetic iron oxide nanoworms with decreased immune recognition and long-circulating properties. ACS Nano. 2014; 8:12437–12449. [PubMed: 25419856]
54. Reynolds F, O'Loughlin T, Weissleder R, Josephson L. Method of determining nanoparticle core weight. Anal Chem. 2005; 77:814–817. [PubMed: 15679348]
55. Bautista MC, Bomati-Miguel O, Morales MD, Serna CJ, Veintemillas-Verdaguer S. Surface characterisation of dextran-coated iron oxide nanoparticles prepared by laser pyrolysis and coprecipitation. J Magn Magn Mater. 2005; 293:20–27.
56. Harpaz Y, Gerstein M, Chothia C. Volume changes on protein folding. Structure. 1994; 2:641–649. [PubMed: 7922041]
57. Quillin ML, Matthews BW. Accurate calculation of the density of proteins. Acta Crystallogr D. 2000; 56:791–794. [PubMed: 10930825]
58. Wisniewski JR, Zougman A, Nagaraj N, Mann M. Universal sample preparation method for proteome analysis. Nat Methods. 2009; 6:359–362. [PubMed: 19377485]
59. Inturi S, et al. Modulatory role of surface coating of superparamagnetic iron oxide nanoworms in complement opsonization and leukocyte uptake. ACS Nano. 2015; 9:10758–10768. [PubMed: 26488074]
60. Forneris F, et al. Structures of C3b in complex with factors B and D give insight into complement convertase formation. Science. 2010; 330:1816–1820. [PubMed: 21205667]

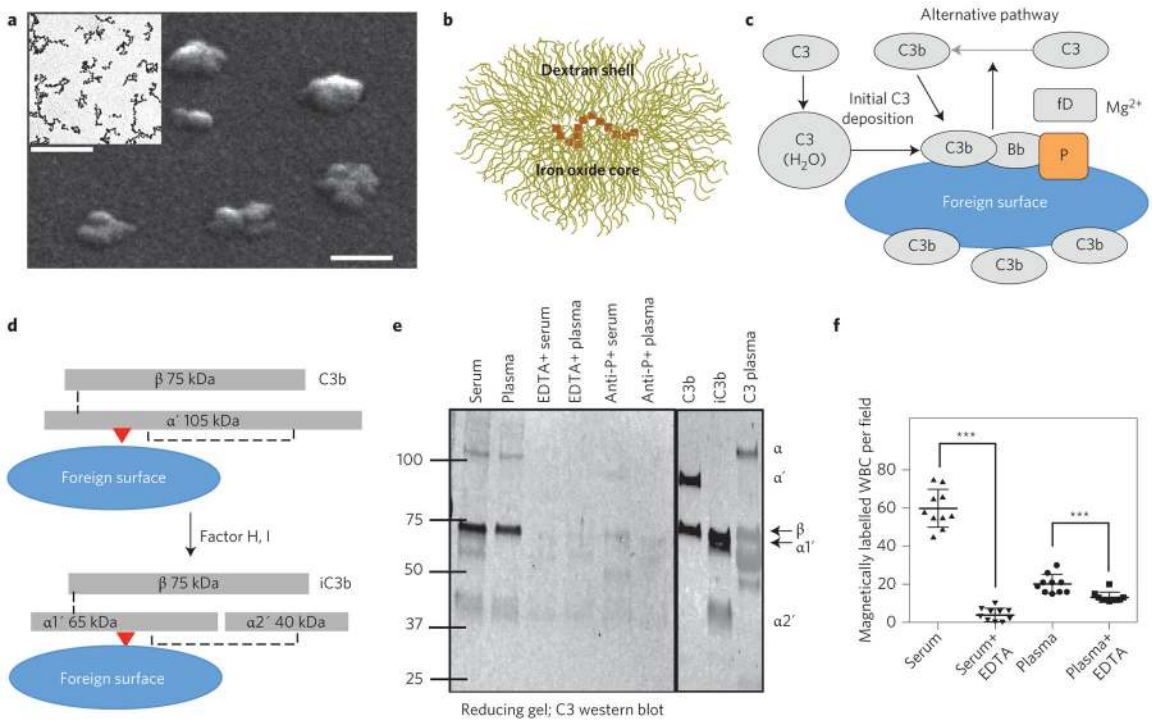

Figure 1. Complement activation and immune uptake of SPIO nanoworms in human serum and plasma

a, Main: FIB–SEM image showing the overall rounded-segmented shape of SPIO nanoworms. Inset: Non-contrast TEM image showing much smaller electron-dense worm-like cores. The dextran shell is not visible on TEM. Scale bars, 200 nm. **b**, Schematic representation of the SPIO nanoworm core–shell structure (based on particle analysis; Supplementary Fig. 1, Supplementary Table 1 and Methods). **c**, Scheme of complement alternative pathway (AP) activation and amplification on a foreign surface. Initially deposited C3b or C3(H_2O) requires factors B, D, properdin (P) and Mg^{2+} to form AP convertase, which activates additional C3 molecules, leading to amplification of C3b opsonization. **d**, C3b covalently binds to the surface and is cleaved by factors H and I, forming iC3b and other degradation products. The dotted line represents the disulfide bridge and the red triangle the covalent bond. **e**, Gel electrophoresis and western blot analysis of C3 opsonization in human serum and plasma. SPIO nanoworms were mixed with serum or plasma, washed, and analysed for C3. Lanes 1–2, serum or plasma only; lanes 3–4, serum or plasma with 10 mM EDTA; lanes 5–6, serum or plasma with anti-properdin (anti-P) antibody; lanes 7–9, purified C3b, iC3b or whole plasma C3. Opsonization was blocked by EDTA (an inhibitor of all complement pathways) or anti-P antibody (an inhibitor of the AP). Detection of a small amount of intact α-chain suggests the presence of C3(H_2O) on the particles. The majority of C3 is in the iC3b form (cleaved α′-chain). The experiment was repeated three times using different sera and plasma. **f**, Assessment of SPIO nanoworm uptake after incubation of opsonized particles with human leucocytes (described in the Methods). The number of magnetically labelled leucocytes (white blood cells (WBC) per microscopic field) was higher in serum than in plasma, and 10 mM EDTA blocked the uptake. Data represent means and s.d. of ten microscopic fields. The experiment was

repeated three times using different sera or plasma. ***$P < 0.001$, non-paired two-sided *t*-test. The data confirm the critical role of AP in C3 opsonization in serum and plasma.

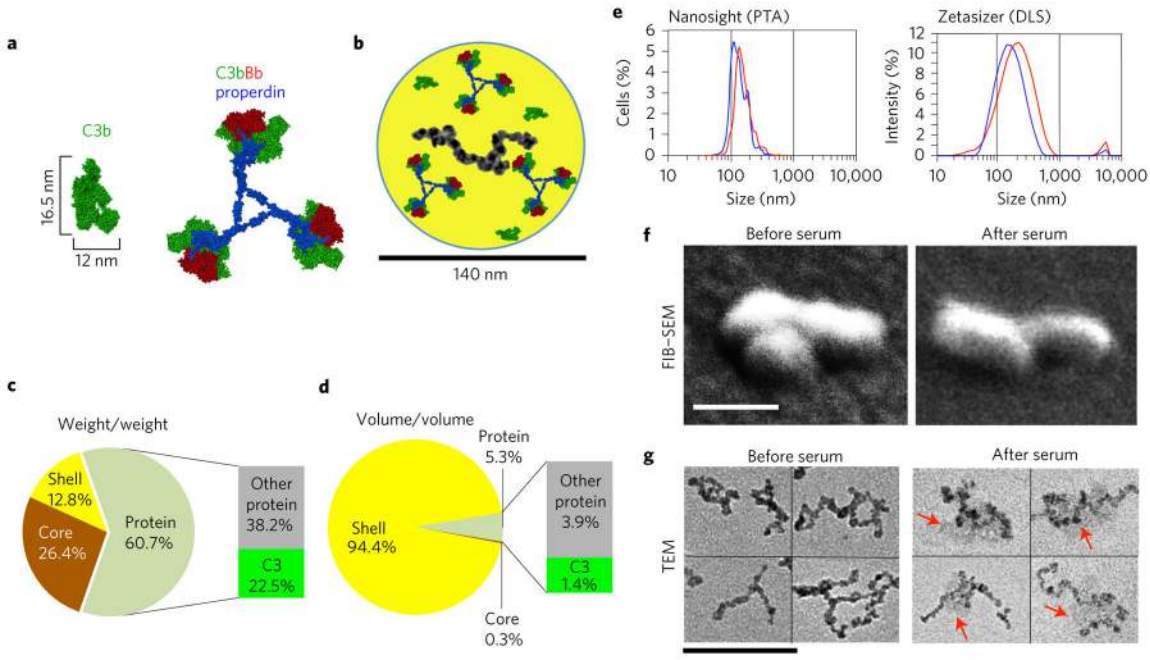

Figure 2. Spatial relationship between complement factors, protein corona and core–shell structure

a, Three-dimensional models of complement C3b and C3bBbP (AP convertase) complex. **b**, Two-dimensional superimposition of the AP factors and a 140-nm-diameter nanoworm (yellow is the dextran shell, black is a TEM image of the worm-like iron oxide core). Multiple C3bBbP complexes and individual C3b molecules can be accommodated within the dextran shell. **c**,**d**, Weight/weight (**c**) and volume/volume (**d**) fractions of serum proteins and complement proteins bound to SPIO nanoworms. For plasma-incubated SPIO nanoworms, the fraction of proteins should be higher due to more absorbed proteins (Supplementary Table 3). Dextran shell occupies the majority of the hydrodynamic volume. For details on calculations see Methods and Supplementary Table 1. **e**, Nanoworms were incubated with serum and washed using a magnetic column. Particle tracking analysis (left) and dynamic light scattering (right) measurements without serum (red trace) and with serum (blue trace) show a slight decrease in particle size. The experiment was repeated twice using sera from different donors. **f**, FIB–SEM images show that nanoworms maintain their overall shape after incubation with serum proteins. Scale bar, 100 nm. **g**, TEM images of SPIO nanoworms before and after incubation with serum and washing. Serum-incubated particles show patchy electron-dense protein clusters (red arrows) close to the iron oxide core. Scale bar, 100 nm. TEM experiments were repeated three times using different sera. These data (together with Supplementary Fig. 4) suggest that complement factors and serum protein corona are probably accommodated in the dextran shell.

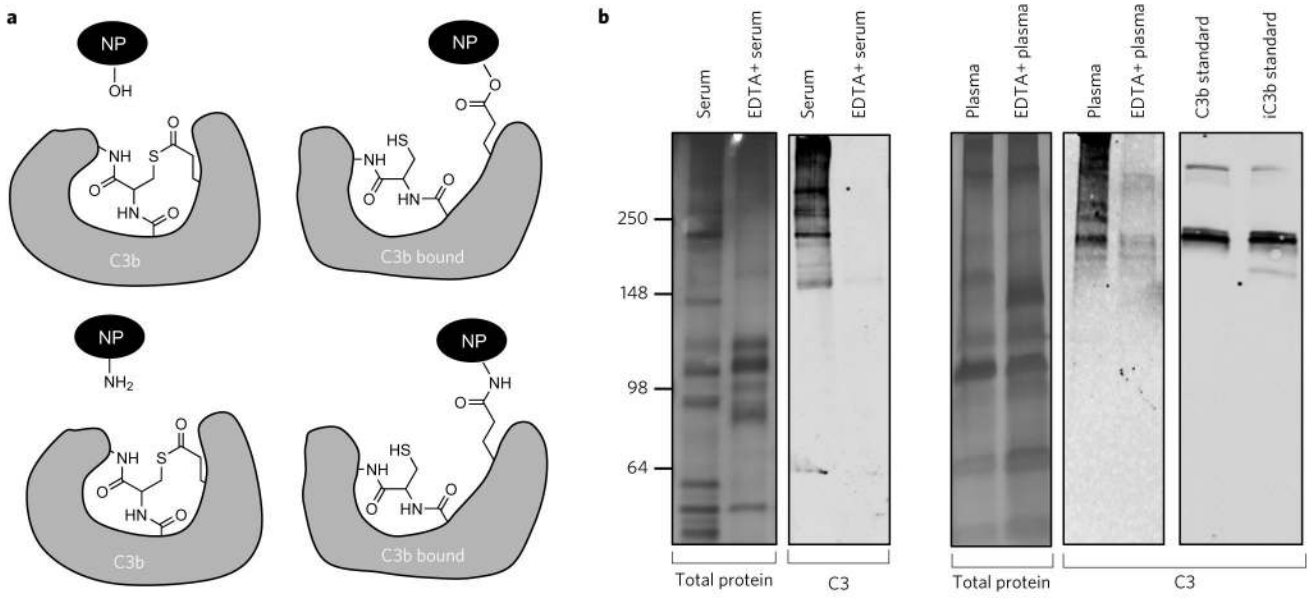

Figure 3. Mechanism of C3 binding to nanoparticles

a, Scheme of C3 fixation on a foreign surface. The active thioester group in C3b can covalently react with hydroxyl or amino groups on the nanoparticle (NP) surface. **b**, Non-reducing gel of proteins bound to nanoparticles in serum or plasma. Following incubation in serum (left) or plasma (right) and washing, proteins were eluted from nanoworms with 2% SDS, separated on a non-reducing SDS–PAGE and analysed for total protein (silver stain) and C3 (western blot). The left lane of each gel shows particles incubated in serum/plasma, and the right lane shows particles incubated with serum/plasma and 10 mM EDTA. The eluted C3 shows a smeared high-molecular-weight pattern (compared to purified C3b/iC3b), suggesting that the majority is bound to the absorbed proteins. EDTA (10 mM) blocks the opsonization of nanoworms with C3, but does not block the binding of other proteins to nanoworms. The experiment was repeated four times using different types of sera/plasma. Plasma panel and C3 standard panel were run on the same gel, but the exposure was adjusted to match the intensities in both panels. A full gel with different exposures is provided in Supplementary Fig. 10. The same mode of C3 binding was observed for plasma protein-coated gold nanoparticles (Supplementary Fig. 6). The data demonstrate that C3 is mostly bound to serum and plasma proteins on the particle surface.

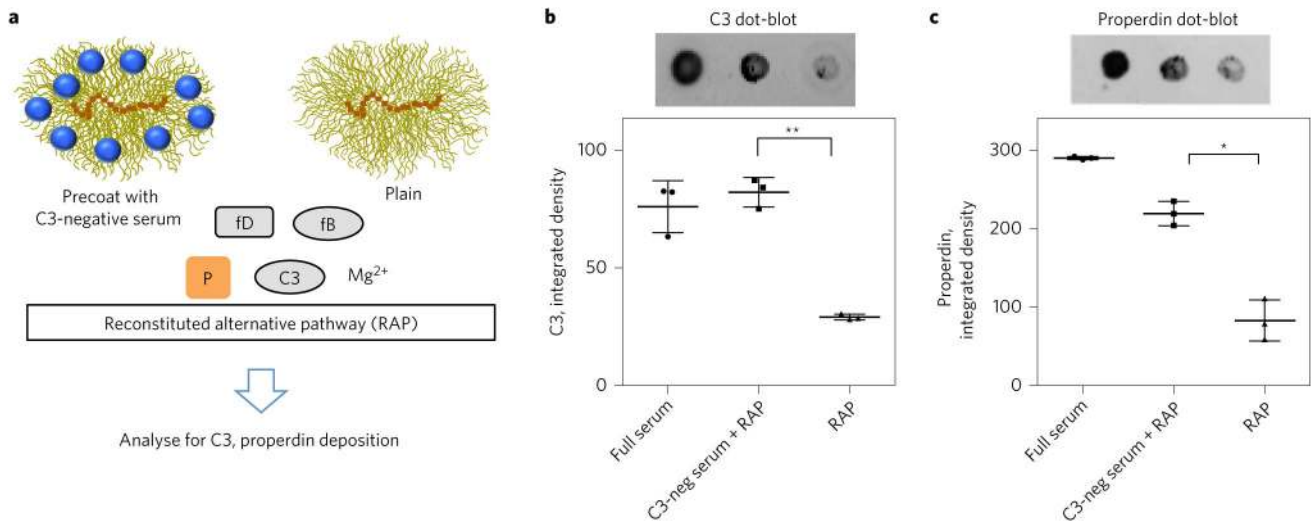

Figure 4. Role of serum protein corona in binding of complement AP factors to SPIO nanoworms

a, SPIO nanoworms precoated with C3-negative human serum (represented by blue spheres) or plain nanoworms were incubated with the reconstituted alternative pathway (RAP) components C3 (0.6 mg ml^{-1}), factor B (100 mg ml^{-1}), properdin (20 μg ml^{-1}) and factor D (10 μg ml^{-1}) in Mg^{2+}-supplemented Veronal buffer[51]. **b**,**c**, C3 and properdin binding was determined with dot-blot immunoassay. There was significantly more binding of complement proteins in the presence of pre-adsorbed serum proteins, suggesting that protein corona facilitates the binding and assembly of complement AP factors. Data show means and s.d., $n = 3$ technical replicates, repeated four times. *$P < 0.05$, **$P < 0.01$, non-paired two-sided t-test.

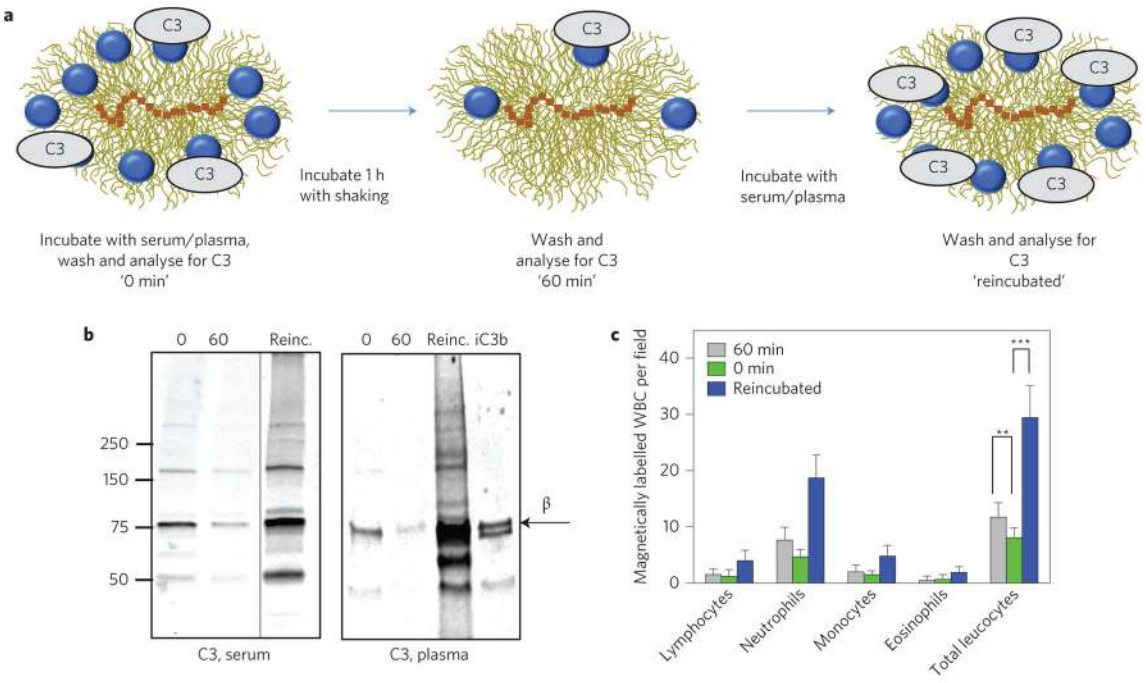

Figure 5. Dynamic behaviour of C3 opsonization *in vitro*

a, SPIO nanoworms were incubated in serum or plasma, washed, incubated with shaking for 60 min, reincubated in fresh serum/plasma from the same donor and washed again. **b**, Western blot analysis of C3 opsonization in serum (left gel) and plasma (right gel) shows loss of C3 after shaking for 60 min and an approximately tenfold increase after reincubation in fresh serum/plasma. The arrow points to the beta chain of C3. In the serum panel, all lanes were run on the same gel. A full gel is provided in Supplementary Fig. 10. **c**, Uptake of SPIO nanoworms, treated as described in **a**, by fresh human leucocytes. Consistent with C3 levels in **b**, there was a significant decrease of uptake after 60 min shaking and enhanced uptake after reincubation in fresh serum. These data demonstrate the dynamic nature of opsonization and the critical role of the exchangeable C3 fraction in the immune uptake. Data show means and s.d., $n = 20$ microscopical fields. The experiment was repeated twice with blood from different healthy donors; $^{***}P < 0.001$, $^{**}P < 0.01$, non-paired two-sided *t*-test.

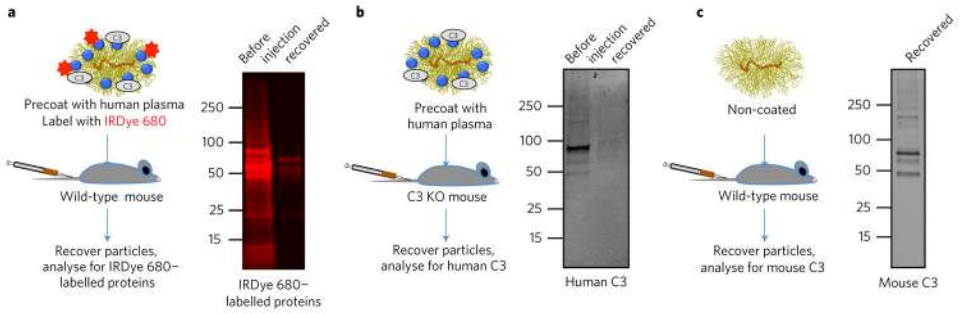

Figure 6. Dynamic behaviour of complement opsonization and protein absorption *in vivo*

a, Loss of absorbed proteins *in vivo*. SPIO nanoworms were precoated with human plasma, quickly labelled with IRDye 680 and injected into wild-type mice. Particles were recovered from blood 5 min post-injection as described in the Methods and analysed for “uorescently labelled proteins. SDS–PAGE shows loss of bound proteins. **b**, Particles were precoated with human plasma, injected into C3-deficient mice and recovered as in the experiment in **a**. Western blot shows loss of C3 *in vivo*. **c**, SPIO nanoworms were injected without precoating into wild-type mouse and recovered as in the experiments in **a** and **b**. Western blot shows fast opsonization with mouse C3 *in vivo*. The same amount of particles before and after injection was loaded on the gel. The data demonstrate rapid loss of C3 and other proteins from particles and rapid opsonization with C3. Experiments were repeated twice.